J|A|C|S
ARTICLES
Published on Web 07/13/2006

# Self-Assembly of Peptide Scaffolds in Biosilica Formation: Computer Simulations of a Coarse-Grained Model

Leonardo Lenoci and Philip J. Camp*

*Contribution from the School of Chemistry, University of Edinburgh, West Mains Road, Edinburgh EH9 3JJ, United Kingdom*

Received February 20, 2006; E-mail: philip.camp@ed.ac.uk

***Abstract:*** The self-assembly of model peptides is studied using Brownian dynamics computer simulations. A coarse-grained, bead−spring model is designed to mimic silaffins, small peptides implicated in the biomineralization of certain silica diatom skeletons and observed to promote the formation of amorphous silica nanospheres in vitro. The primary characteristics of the silaffin are a 15 amino acid hydrophilic backbone and two modified lysine residues near the ends of the backbone carrying long polyamine chains. In the simulations, the model peptides self-assemble to form spherical clusters, networks of strands, or bicontinuous structures, depending on the peptide concentration and effective temperature. The results indicate that over a broad range of volume fractions (0.05−25%) the characteristic structural lengthscales fall in the range 12−45 nm. On this basis, we suggest that self-assembled structures act as either nucleation points or scaffolds for the deposition of 10−100 nm silica−peptide building blocks from which diatom skeletons and synthetic nanospheres are constructed.

## 1. Introduction

One of the major goals in materials chemistry is to devise methods for the controlled fabrication of complex structures from simple inorganic materials. Aside from being of considerable inherent interest, the ability to construct architectures on the nanoscale would provide a means of producing devices for technological applications. In developing appropriate synthetic strategies, it is becoming commonplace to look for inspiration from Nature and how she controls biomineralization.[1] The most abundant biominerals are calcium carbonate and silica, with most siliceous materials being found in marine single-cell organisms such as diatoms and radiolaria.[2,3] Diatom cell walls (frustules) exhibit a variety of complex porous architectures on the 10 nm to 10 $\mu$m lengthscale, made from composites of hydrated $SiO_2$ and biopolymers. Atomic force and scanning electron microscope images of diatom frustules indicate that the fundamental building blocks are tightly packed spheres, with diameters in the region of 10−100 nm.[4−8]

At this early stage in the study of biomineralization at the molecular scale, it is necessary to focus on some specific examples before attempting to identify connections between seemingly disparate systems. There is a vast number of diatom species to survey, but the past decade has seen some significant advances. Therefore, for the purpose of this article, we can give only a brief summary of a particular set of experiments. In a series of exciting papers, Sumper and co-workers have explored the detailed structure and properties of biosilica extracted from a range of diatom species. For example, the frustule of the diatom *Cylindrotheca fusiformis* was found to contain significant amounts of organic material which includes characteristic proteins called "silaffins",[9] and long-chain polyamines (LCPAs).[10] There are other components present, but these are known to associate with biosilica only after deposition is complete.[11,12] Three main silaffin fractions were identified with molecular weights of 4 kDa (silaffin 1A), 8 kDa (silaffin 1B), and 17 kDa (silaffin 2). Silaffin 1A itself was found to consist of a mixture of two peptides—designated $1A_1$ and $1A_2$—with very similar primary structures. The primary structure of silaffin $1A_1$ contains serine (S), lysine (K), glycine (G), and tyrosine (Y) residues: SSKKSGSYSGSKGSK. The serines are phosphorylated, whereas the lysines at positions 3 and 15 are each posttranslationally modified with a polyamine tail containing 5−10 *N*-methylpropylamine [$-(CH_2)_3 - N(CH_3)-$] units connected to the backbone by a link of propylamine [$-(CH_2)_3 - NH-$] units; see Figure 1c of ref 13.

Silaffins are implicated in the formation of the complex porous structures in diatom frustules, and so it was of interest to find out whether silaffins can promote silica formation in vitro from a suitable precursor. The addition of silaffin 1A (0.1−

(1) Mann, S.; Ozin, G. A. *Nature* **1996**, *382*, 313−318.
(2) Volcani, B. E.; Simpson, T. L. *Silicon and siliceous structures in biological systems*; Springer: Berlin, 1981.
(3) Lowenstam, H. A.; Weiner, S. *On Biomineralization*; Oxford University Press: Oxford, 1989.
(4) Chiappino, M. L.; Volcani, B. E. *Protoplasma* **1977**, *93*, 205−221.
(5) Schmid, A. M. M.; Schulz, D. *Protoplasma* **1979**, *100*, 267−288.
(6) Cox, E. J. *J. Phycol.* **1999**, *35*, 1297−1312.
(7) Crawford, S. A.; Higgins, M. J.; Mulvaney, P.; Wetherbee, R. *J. Phycol.* **2001**, *37*, 543−554.
(8) Noll, F.; Sumper, M.; Hampp, N. *Nano Lett.* **2002**, *2*, 91−95.
(9) Kröger, N.; Deutzmann, R.; Sumper, M. *Science* **1999**, *286*, 1129−1132.
(10) Kröger, N.; Deutzmann, R.; Bergsdorf, C.; Sumper, M. *Proc. Natl. Acad. Sci. U.S.A.* **2000**, *97*, 14133−14138.
(11) van de Poll, W. H.; Vrieling, E. G.; Gieskes, W. W. C. *J. Phycol.* **1999**, *35*, 1044−1053.
(12) Kröger, N.; Wetherbee, R. *Protist* **2000**, *151*, 263−273.
(13) Kröger, N.; Lorenz, S.; Brunner, E.; Sumper, M. *Science* **2002**, *298*, 584−586.

10.1021/ja061211s CCC: $33.50 

0.5 mM) to ~1 M silicilic acid at pH > 3 yields a precipitate of silica spheres with diameters in the range 400−700 nm.[9,13] These dimensions are not biologically relevant, but time-resolved studies suggest that the early stages of biosilica formation lead to a moldable silica−silaffin composite from which large spheres emerge as a result of subsequent artificial processes.[13] Silaffin 2 appears to play a regulatory role,[14] whereas LCPAs from a range of biological species are known to promote nanopatterned silica formation.[10,15] In the case of the genus *Coscinodiscus*, the formation of a hierarchical hexagonal silica frustule is thought to be driven by the phase separation and droplet formation of LCPAs in water, which would suggest that the LCPAs are somewhat hydrophobic.[16] (A separate computational test of this "phase-separation" model is currently in progress.) Recent work indicates that the self-assembly of LCPAs might be promoted by specific anionic additives—such as phosphates—providing bridges between (protonated) nitrogen centers.[17,18] The roles of amine groups in the acid−base chemistry of silica condensation have also been noted.[19] A review of experiments on silaffins and LCPAs in the context of silica formation can be found in ref 20.

At this point we briefly mention that silica deposition can also be effected by a silaffin-type peptide without the post-translational, polyamine tail modification.[9,21−23] Nonmodified peptide R5 is made up of 19 amino acids, forming the silaffin $1A_1$ backbone plus two arginines (R), an isoleucine (I), and a leucine (L) appended to the C-terminus. The RRIL motif has been shown to be crucial for silica deposition and to the formation of aggregates.[23] It has been suggested that the close proximity of the charged arginine residues to the hydrophobic isoleucine and leucine residues leads to the self-assembly of micelle-like structures; the R5 backbone without the RRIL motif shows almost no silica deposition and no aggregate formation.[23] This indicates that the polyamine tails on silaffins are crucial for aggregate formation.

In this article, we make the first simulation-led attack on the problem of how silaffins alone might promote the formation of 10−100 nm silica−peptide composites. As with all such phenomena, it is tempting to speculate that the peptides self-assemble to form some sort of scaffold around which an (as yet unknown) precursor can deposit silica.[24−27] Indeed, the analogies between the formation of porous biominerals, and the synthetic templating of microporous and mesoporous solids,[28,29] appear all too obvious. The fact that silaffin 1A alone can precipitate silica suggests that it possess an inherent ability to self-assemble.[13] The silaffin peptide backbone comprises polar amino acids, and the serines are phosphorylated; hence, this will be a strongly hydrophilic unit due to the opportunity for electrostatic and hydrogen-bonding interactions with water. We propose that self-assembly is driven by an effective attraction between the polyamine tails, arising either from a solubility mismatch between the tails and the backbone or from a phosphate-bridging mechanism, as explained below.

The tertiary amine groups—once protonated—represent the only hydrophilic components of the polyamine tails. The p$K_a$ for the conjugate acid of an isolated tertiary amine group is usually around 9,[30] but the close proximity of other protonation sites within the polyamine tails will significantly reduce the probability of many sites on the same tail being protonated under near-neutral conditions. To get an idea of the magnitude of this effect, consider *N*,*N*,*N*′,*N*′-tetramethyl-1,3-propanediamine, $(CH_3)_2N(CH_2)_3N(CH_3)_2$, for which the p$K_a$ of the singly protonated molecule is 9.76 and that of the doubly protonated molecule is 7.53.[31] Assessing the degree of protonation at anything but infinite dilution is not straightforward due to the role of activity coefficients, but this effect combined with the presence of the absolutely hydrophobic propyl and methyl units may limit the extent to which the polyamine tails can compete with the peptide backbone for contact with the solvent. (Indeed, a protonated propylamine unit by itself may possess amphiphilic characteristics; even small polar molecules, such as methanol and ethanol, do not fully mix with water on the molecular scale.[32]).

Phosphate-bridging mechanisms have also been proposed to explain the apparent tendency for polyamine chains to aggregate.[15,17,18] Experiments on polyallylamines with molecular weights in the region of 15 kDa show that the formation of aggregates is strongly dependent on the concentration of phosphate anions[15] and on the pH.[18] Different anions do not facilitate aggregation, and so it is likely that there is a specific hydrogen-bonding mechanism for the cross-linking of the polyamine tails. Similar observations have been made with dephosphorylated silaffins[13] and poly(L-lysine).[17] Returning to silaffins, it is therefore possible that the phosphorylated backbone provides the necessary bridging phosphate groups to mediate an effective attraction between the polyamine tails. In ref 13, Kröger et al. "conclude that the numerous phosphate groups in [natural silaffin 1A] serve as an intrinsic source of anions required for silica formation by diatoms".

In summary, experiments on silaffins, and on pure polyamines, suggest that there is an effective attraction between the polyamine units, driving self-assembly and hence scaffold formation. To explore the implications of these effects, it would be preferable to obtain simulation results for an atomistically detailed representation of silaffins in solution. For the sizes of molecules under consideration here, and the lengthscales (up

(14) Poulsen, N.; Sumper, M.; Kröger, N. *Proc. Natl. Acad. Sci. U.S.A.* **2003**, *100*, 12075−12080.
(15) Brunner, E.; Lutz, K.; Sumper, M. *Phys. Chem. Chem. Phys.* **2004**, *6*, 854−857.
(16) Sumper, M. *Science* **2002**, *295*, 2430−2433.
(17) Rana, R. K.; Murthy, V. S.; Yu, J.; Wong, M. S. *Adv. Mater.* **2005**, *17*, 1145−1150.
(18) Lutz, K.; Gröger, C.; Sumper, M.; Brunner, E. *Phys. Chem. Chem. Phys.* **2005**, *7*, 2812−2815.
(19) Patwardhan, S. V.; Clarson, S. J.; Perry, C. C. *Chem. Commun.* **2005**, 1113−1121.
(20) Sumper, M.; Kröger, N. *J. Mater. Chem.* **2004**, *14*, 2059−2065.
(21) Brott, L. L.; Naik, R. R.; Pikas, D. J.; Kirkpatrick, S. M.; Tomlin, D. W.; Whitlock, P. W.; Clarson, S. J.; Stone, M. O. *Nature* **2001**, *413*, 291−293.
(22) Naik, R. R.; Whitlock, P. W.; Rodriguez, F.; Brott, L. L.; Glawe, D. D.; Clarson, S. J.; Stone, M. O. *Chem. Commun.* **2003**, 238−239.
(23) Knecht, M. R.; Wright, D. W. *Chem. Commun.* **2003**, 3038−3039.
(24) Mann, S. *J. Chem. Soc., Dalton Trans.* **1997**, 3953−3961.
(25) Mann, S.; Davis, S. A.; Hall, S. R.; Li, M.; Rhodes, K. H.; Shenton, W.; Vaucher, S.; Zhang, B. *J. Chem. Soc., Dalton Trans.* **2000**, 3753−3763.
(26) Dabbs, D. M.; Aksay, I. A. *Annu. Rev. Phys. Chem.* **2000**, *51*, 601−622.
(27) Patwardhan, S. V.; Mukherjee, N.; Steinitz-Kannan, M.; Clarson, S. J. *Chem. Commun.* **2003**, 1122−1123.
(28) Kresge, C. T.; Leonowicz, M. E.; Roth, W. J.; Vartuli, J. C.; Beck, J. S. *Nature* **1992**, *359*, 710−712.
(29) Beck, J. S.; Vartuli, J. C.; Roth, W. J.; Leonowicz, M. E.; Kresge, C. T.; Schmitt, K. D.; Chu, C. T.-W.; Olson, D. H.; Sheppard, E. W.; McCullen, S. B.; Higgins, J. B.; Schlenker, J. L. *J. Am. Chem. Soc.* **1992**, *114*, 10834−10843.
(30) De Robertis, A.; Foti, C.; Giuffrè, O.; Sammartano, S. *J. Chem. Eng. Data* **2001**, *46*, 1425−1435.
(31) Näsänen, R.; Tilus, P.; Teikari, T. *Finn. Chem. Lett.* **1974**, 263−265.
(32) Dixit, S.; Crain, J.; Poon, W. C. K.; Finney, J. L.; Soper, A. K. *Nature* **2002**, *416*, 829−832.

to hundreds of nanometers) being probed in experiments, this is not a realistic proposition. We therefore seek a coarse-grained model that includes the essential characteristics of real molecules and ignores any irrelevant molecular detail. We might model the silaffins as polyelectrolytes, but in the absence of concrete evidence about the degree and pattern of protonation on the polyamine tails, not to mention the possibility that "covalent" bonding may be important, it would seem premature to follow this path. On the basis of the physical arguments offered above, we have constructed model silaffins consisting of strongly hydrophilic peptide backbones, decorated with mutually attractive flexible tails. The coarse-grained model is obtained from a "bead−spring" approach, which originated in simulations of polymer blends and block copolymers.[33] Each "bead" represents the average shape of a group of atoms, and the beads are connected with "springs" in such a way as to mimic the essential structural characteristics of the molecule. Bead−spring models continue to find application in a vast range of complex-fluid problems, including block copolymers, surfactants, polypeptides, and polyelectrolytes. The model we describe in section 2 resembles those of certain gemini amphiphiles and (bio)-polymers[34−36] which have been studied with coarse-graining approaches.

Given the coarse-grained bead−spring model, we use Brownian dynamics (BD) simulations to assemble and characterize molecular aggregates that might be formed and therefore identify putative structural templates for biosilica spheres. In what follows, we will show that the characteristic lengthscales of the self-assembled structures are in the range 12−45 nm, i.e., comparable to the sizes of natural biosilica building blocks.[4−8] Encouraged by the accord of our simulation results with experimental observations, we then go on to speculate as to the role of structure-directing peptides, such as silaffins, in the formation of biosilica.

This article is organized as follows. Details of the model and the simulation methodology will be presented in section 2. Results are presented and discussed in section 3, and section 4 concludes the paper.

## 2. Model and Simulation Methods

The silaffin backbone consists of 15 amino acids. In *crystals*, the average spacing between amino acids in an elongated $\beta$-strand is ∼0.35 nm. Due to the high concentration of phosphorylated serine residues, it is unlikely that the backbone will form a more compact α-helix in solution; thus, for the order-of-magnitude calculations presented below, we estimate that the length of the backbone is ∼6 nm. We represent the backbone with three hydrophilic "head" (H) beads, linked by finitely extensible nonlinear elastic (FENE) springs[37] to be defined below. The silaffin tails typically consist of ∼10 propylamine units. Assuming C−C and C−N bond lengths of ∼0.15 nm, the length of a tail will be roughly comparable with the length of the backbone. Hence, we represent each chain by three tail (T) beads, again linked by FENE springs. The resulting molecular structure is illustrated in Figure 1. For purposes of comparison with experimental parameters below, the bead diameter is roughly equal to 2 nm.

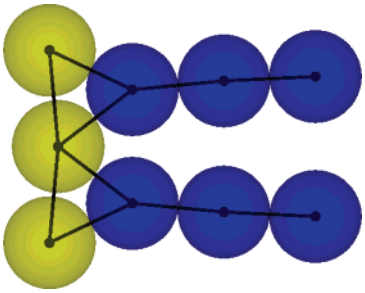

***Figure 1.*** Molecular model considered in this work. The yellow beads represent the peptide backbone, and the blue beads represent the polyamine tails. The FENE springs are shown as black lines connecting the beads.

The bead−bead interactions are defined in terms of the Lennard-Jones (LJ) potential

$$u_{\mathrm{LJ}}(r) = 4\epsilon\left[\left(\frac{\sigma}{r}\right)^{12} - \left(\frac{\sigma}{r}\right)^{6}\right] \tag{1}$$

where $\epsilon$ is the well depth, and $\sigma$ is the bead diameter. The head−head (HH) interaction potential is taken to be

$$u_{\mathrm{HH}}(r) = \begin{cases} u_{\mathrm{LJ}}(r) - u_{\mathrm{LJ}}(r_0) & r \le r_0 \\ 0 & r > r_0 \end{cases} \tag{2}$$

where $r_0 = 2^{1/6}\sigma$ is the position of the minimum in the LJ potential. The potential coincides with the Weeks−Chandler−Andersen potential.[38] It is purely repulsive, and in this case reflects the assumption that the components of the hydrophilic backbone are ambivalent toward solvation and mutual interaction. The tail−tail (TT) interaction potential must include an attractive portion, to promote aggregation:

$$u_{\mathrm{TT}}(r) = \begin{cases} u_{\mathrm{LJ}}(r) - u_{\mathrm{LJ}}(r_c) & r \le r_c \\ 0 & r > r_c \end{cases} \tag{3}$$

The cutoff distance is taken to be $r_c = 2.5\sigma$; the resulting cut-and-shifted potential is almost identical with the full LJ potential, and is continuous at $r = r_c$. The head−tail (HT) interaction potential is taken to be the same as that for the HH interaction, i.e., $u_{\mathrm{HT}}(r) = u_{\mathrm{HH}}(r)$ (2). The FENE spring potential linking each bead to its neighbor(s) is

$$u_{\mathrm{FENE}}(r) = -\frac{1}{2}kR_0^2 \ln\left[1 - \left(\frac{r}{R_0}\right)^2\right] \tag{4}$$

where $k = 30\epsilon\sigma^{-2}$ is the spring constant and $R_0 = 1.5\sigma$ is the maximum allowable separation between bonded beads.[37]

With a cutoff distance of $r_c = 2.5\sigma$, the range of $u_{\mathrm{TT}}(r)$ is comparable with the bead diameter. At first glance, this situation appears somewhat unrealistic because each bead (representing several functional groups) has dimension ∼2 nm, while direct interatomic forces are limited to the subnanometer range. It must be remembered, however, that coarse-grained "potentials" are really free energies, resulting from an integration over the solvent degrees of freedom, with the beads held fixed. Therefore, the interaction range is not restricted to those of interatomic forces; it should be extended to accommodate longer-range, solvent-mediated effects such as hydrophobic attraction.[39]

BD simulations[40] of $N_m = 300$ or $N_m = 600$ molecules (corresponding to $N_b = 2700$ and $N_b = 5400$ beads, respectively) were carried out in a cubic simulation cell of volume $V = L^3$ with periodic boundary conditions applied. The masses of all beads were set equal to $m$.

(33) Grest, G. S.; Lacasse, M.-D.; Kremer, K.; Gupta, A. M. *J. Chem. Phys.* **1996**, *105*, 10583−10594.
(34) Maiti, P. K.; Lansac, Y.; Glaser, M. A.; Clark, N. A. *Langmuir* **2002**, *18*, 1908−1918.
(35) Kim, K. H.; Kim, S. H.; Huh, J.; Jo, W. H. *J. Chem. Phys.* **2003**, *119*, 5705−5710.
(36) Guo, L.; Luijten, E. *J. Polym. Sci. B* **2005**, *43*, 959−969.
(37) Grest, G. S.; Kremer, K. *Phys. Rev. A* **1986**, *33*, 3628−3631.
(38) Weeks, J. D.; Chandler, D.; Andersen, H. C. *J. Chem. Phys.* **1971**, *54*, 5237−5247.
(39) Lum, K.; Chandler, D.; Weeks, J. D. *J. Phys. Chem. B* **1999**, *103*, 4570−4577.
(40) Allen, M. P.; Tildesley, D. J. *Computer simulation of liquids*; Clarendon Press: Oxford, 1987.

The equation of motion of bead $i$ is

$$m\ddot{\mathbf{r}}_i = -\nabla_i U - m\xi\,\dot{\mathbf{r}}_i + \mathbf{R}_i \quad (5)$$

where $\mathbf{r}_i$ is the position vector of bead $i$, $U$ is the potential energy (given by an appropriate sum over pairs of beads and bonds), $\xi$ is the friction coefficient, and $\mathbf{R}_i$ is a stochastic force, representing the influence of the solvent. The latter term is represented by Gaussian white noise, subject to the fluctuation−dissipation relation $\langle \mathbf{R}_i(t)\cdot\mathbf{R}_j(t')\rangle = 6mk_BT\xi\delta_{ij}\delta(t - t')$. The equations of motion were integrated using a velocity-Verlet-like algorithm.[40] The reduced time step was set equal to $\delta t = 0.01\tau$, where $\tau = \sqrt{m\sigma^2/\epsilon}$ is the basic unit of time. The reduced friction coefficient was $\xi = 5\tau^{-1}$, which represents damped dynamics appropriate to the large chemical units being represented by each bead. The reduced bead density is $\rho^* = N_b\sigma^3/V$, and the volume fraction is $\phi = \pi\rho^*/6$. The strength of the bead−bead interaction is measured by the reduced temperature $T^* = k_BT/\epsilon$, where $k_B$ is Boltzmann's constant. On thermodynamic grounds, $T^*$ must be at most on the order of 1 for self-assembly to occur so that the effective attraction may overcome the entropy penalty associated with clustering.

For each state point considered, we carried out equilibration and production runs consisting of $\sim 10^5$ time steps. Equilibration was assessed by comparing energies and cluster distribution functions (section 3.2) from four independent runs with different initial configurations and random-number generator seeds (for the stochastic force part). For low densities $\rho^* \leq 0.1$, systems of $N_m = 300$ molecules were sufficiently large to accommodate the self-assembled structures that emerged. At higher densities ($\rho^* = 0.3$, 0.5) systems of $N_m = 600$ molecules were studied in addition to check for finite-size effects (which were found to be insignificant). In each case, initial configurations were well equilibrated at high temperature ($T^* \sim 5$).

## 3. Results and Discussion

Test runs at high temperatures $T^* > 1$ showed no significant signs of self-assembly. Runs at low temperatures $T^* < 0.5$ exhibited self-assembled structures, but the equilibration and relaxation were extremely sluggish, and required prohibitively long simulations. We therefore concentrated on two temperatures between these extremes, $T^* = 0.5$ and $T^* = 0.8$. We first describe the qualitative aspects of self-assembly in the model system (section 3.1). We then characterize cluster formation at low densities (section 3.2), and other structural aspects at higher densities as evidenced by the static structure factor and transient (silaffin-free) cavities in the model fluid (section 3.3).

**3.1. Self-Assembly.** In Figure 2 we show final configurations at a representative selection of densities, and at temperatures of $T^* = 0.5$ and $T^* = 0.8$. At low densities ($\rho^* \leq 0.1$) distinct aggregates resembling micelles are in evidence. An analysis of the cluster distribution is presented in section 3.2. At higher densities ($\rho^* = 0.3$, 0.5) the fluid is characterized by extended networks of elongated structures that locally resemble bilayers or wormlike micelles, with the polyamine tails interdigitated. The overall gel-like structure possesses numerous cavities, which of course would be occupied by solvent and silica precursor in the real system. These structures are vaguely reminiscent of those observed in simulations of gemini surfactants,[34] and the extended networks of triblock-surfactant templates.[41] The characteristic structural lengthscale, and the distribution of cavity sizes, will be considered in section 3.3. Self-assembled structures are essentially absent at temperatures above $T^* = 1$, and at densities above $\rho^* = 0.5$.

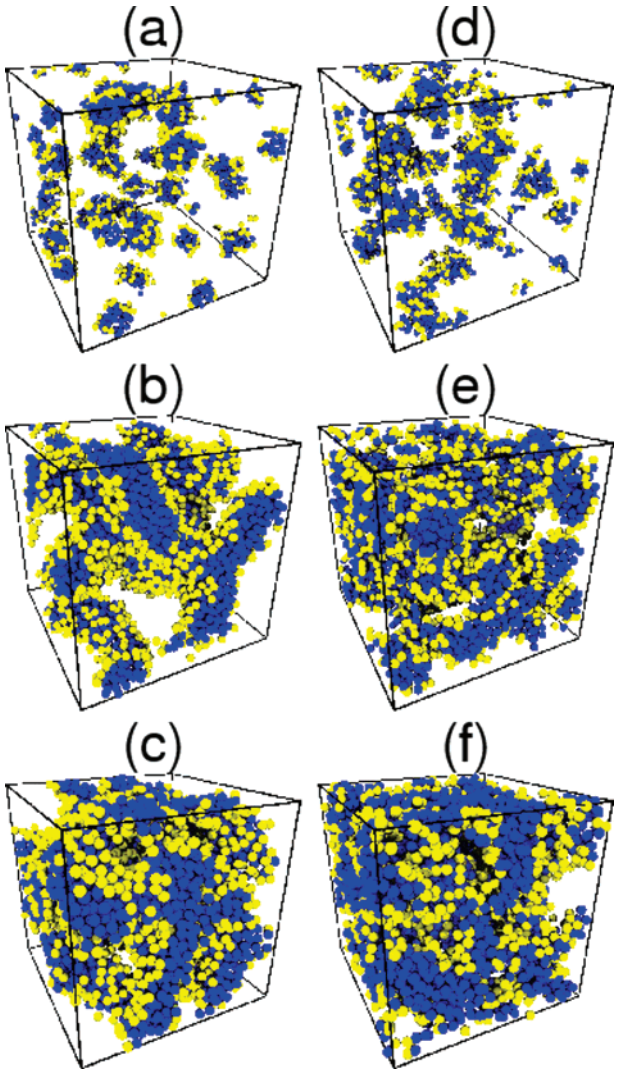


***Figure 2.*** Simulation configurations after equilibration: (a) $T^* = 0.5$, $\rho^* = 0.06$; (b) $T^* = 0.5$, $\rho^* = 0.3$; (c) $T^* = 0.5$, $\rho^* = 0.5$; (d) $T^* = 0.8$, $\rho^* = 0.06$; (e) $T^* = 0.8$, $\rho^* = 0.3$; (f) $T^* = 0.8$, $\rho^* = 0.5$. System sizes at $\rho^* = 0.06$ are $N_m = 300$ molecules, while those at $\rho^* = 0.3$ and $\rho^* = 0.5$ are $N_m = 600$ molecules.

**3.2. Structure at Low Density ($\rho^* \leq 0.1$).** Cluster formation at low densities ($\rho^* \leq 0.1$) was explored by computing the volume fraction of clusters containing $n$ molecules, $\phi_n$. If any two mutually attracting tail beads on two different molecules were within a cutoff distance $r_{tail} = 1.5\sigma$, then those two molecules were deemed to belong to the same cluster.[42,43] (An alternative cluster criterion will be discussed below.) The overall degree of aggregation at a given temperature was monitored by plotting the volume fraction of free molecules ($\phi_1$) against the total volume fraction ($\phi$), as shown in Figure 3. At very low concentrations, we see that $\phi_1 \approx \phi$, as should be expected when there is little or no aggregation. At $T^* = 0.5$ the free-molecule concentration reaches a peak at a total volume fraction $\phi \simeq 0.008$, while at $T^* = 0.8$ the peak occurs at $\phi \simeq 0.01$; we loosely identify the positions of these peaks as the critical 'micelle' concentrations.[44] At higher concentrations, the clusters

(41) Bhattacharya, S.; Gubbins, K. E. *J. Chem. Phys.* **2005**, *123*, 134907.
(42) Smit, B.; Hilbers, P. A. J.; Esselink, K.; Rupert, L. A. M.; van Os, N. M.; Schlijper, A. G. *J. Phys. Chem.* **1991**, *95*, 6361−6368.
(43) von Gottberg, F. K.; Smith, K. A.; Hatton, T. A. *J. Chem. Phys.* **1997**, *106*, 9850−9857.
(44) Israelachvili, J. *Langmuir* **1994**, *10*, 3774−3781.

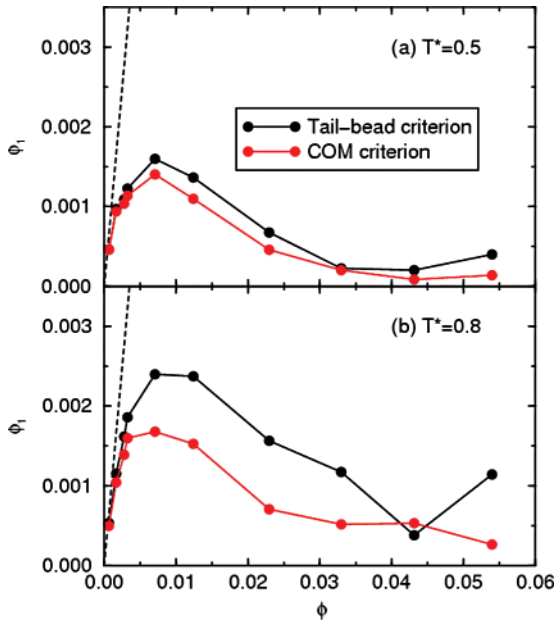


***Figure 3.*** Volume fraction of free monomers ($\phi_1$) against total volume fraction ($\phi$) at temperatures (a) $T^* = 0.5$ and (b) $T^* = 0.8$. The black points represent the tail-bead distance criterion, and the red points represent the molecular center-of-mass distance criterion (see text). The dashed lines represent the asymptotic, low-density dependence $\phi_1 = \phi$.

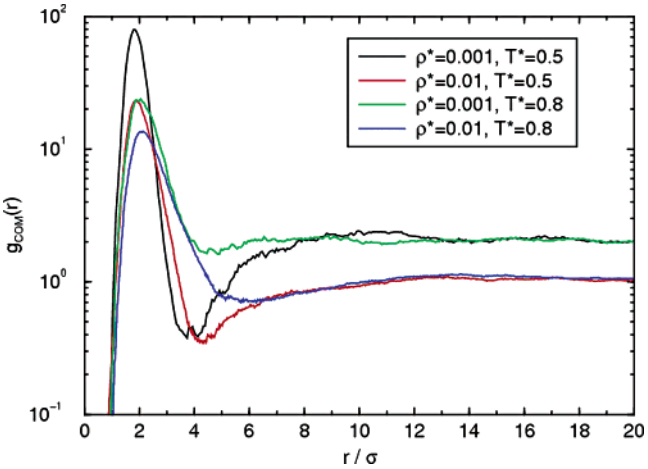


***Figure 4.*** Center-of-mass radial distribution functions, $g_{COM}(r)$ at $\rho^* = 0.001$, $T^* = 0.5$ (black); $\rho^* = 0.01$, $T^* = 0.5$ (red); $\rho^* = 0.001$, $T^* = 0.8$ (green); and $\rho^* = 0.01$, $T^* = 0.8$ (blue). The curves for $\rho^* = 0.001$ (green and black) approach $g_{COM}(r) = 1$ at $r >> 20\sigma$ (not shown).

coalesce to form larger aggregates, and ultimately structures that span the simulation cell.

An important technical question is how to identify clusters unambiguously, and in a physical meaningful way. Thus far, our definition has been based on a tail-bead distance criterion, in line with earlier work.[42,43] In the case of molecules with very long tails, however, this criterion becomes necessary but not sufficient to identify two monomers belonging to the same aggregate; just two beads in close proximity may not be sufficient to bind the molecules together. We therefore tested an alternative criterion based on the separation of the molecular centers-of-mass (COMs). To establish a suitable cutoff distance, we first computed the center-of-mass radial distribution function, $g_{COM}(r)$.[40] In Figure 4 we plot $g_{COM}(r)$ for systems at various densities and temperatures. The peaks centered at $r \simeq 2\sigma$ signal aggregated pairs of molecules. Minima occur in the range $r = 4-6\sigma$ and provide natural criteria for discriminating between aggregated and free pairs of molecules. We implemented the COM cluster criterion with a cutoff of $r_{COM} = 5\sigma$; the results for $\phi_1$ versus $\phi$ are compared with those using the conventional tail-bead criterion in Figure 3. The two criteria yield very similar results at low concentrations, which is comforting because there the clusters are quite distinct (see Figure 2). At higher concentrations, the COM criterion yields a smaller number of free monomers, particularly so at the higher temperature ($T^* = 0.8$). One explanation is that at high concentrations and high temperatures, the centers-of-mass of two molecules can be in close proximity simply due to confinement, and without the tail-beads being within interaction range. Despite this minor discrepancy, the general trends in Figure 3 are insensitive to the cluster criterion, and hence our estimates of the critical micelle concentrations are unaltered.

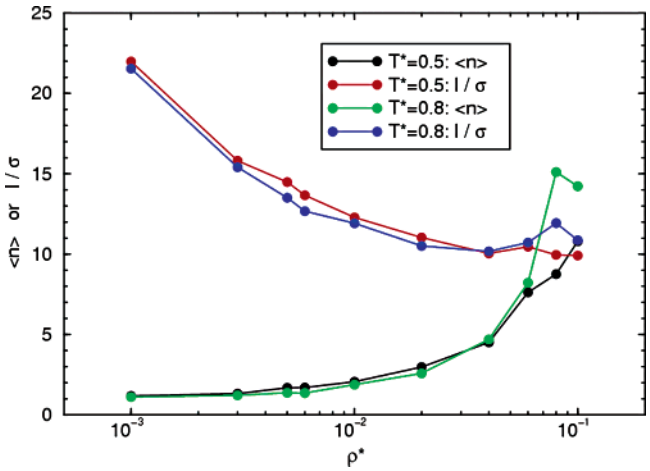


***Figure 5.*** Average number of molecules per cluster ($\langle n \rangle$) and average cluster separation ($l/\sigma$) at $T^* = 0.5$ (black and red, respectively) and $T^* = 0.8$ (green and blue, respectively).

One of the objectives of this study is to identify characteristic structural lengthscales that might correlate with the sizes of the silica building blocks found in diatom skeletons. In the low-density regime currently under consideration, one key dimension is the average separation between neighboring clusters, which we denote by $l$. We first need to calculate the average cluster density: since there are 9 beads per molecule, this quantity is equal to $\rho^*/9\langle n \rangle$, where $\langle n \rangle$ is the average number of molecules per cluster. In reduced units, $l$ is then given by

$$\frac{l}{\sigma} = \left(\frac{9\langle n \rangle}{\rho^*}\right)^{1/3} \qquad (6)$$

In Figure 5 we show $\langle n \rangle$ (from the tail-bead criterion) and $l/\sigma$ as functions of density along the isotherms $T^* = 0.5$ and $T^* = 0.8$. The average cluster size $\langle n \rangle$ grows with increasing concentration, and above $\rho^* = 0.1$ all molecules in the system belong to the same aggregate. The mean separation between clusters decreases monotonically with increasing density and then appears to level off at around $10\sigma$. In this density regime, it is tempting to ask whether the formation of silica spheres is initiated on the surfaces of clusters or even, at very low densities, from a single peptide. In this scenario, the silica spheres might grow out radially from spherical nuclei until they come in contact, and so the sphere size would be dictated by the mean separation between neighboring clusters. From Figure 5 we see

that over a wide range of volume fraction ($0.05\% \leq \phi \leq 5\%$), the mean separation varies relatively little; with $\sigma \simeq 2$ nm, the silica-sphere diameter would be between 20 and 45 nm. This is in excellent agreement with the dimensions of the silica building blocks seen in experiments;[4−8] however, without knowing the real volume fraction of peptide in diatom cells, it is impossible to tell whether this nucleation mechanism is reasonable. It would be very useful to know how the organic components are distributed within the silica building blocks found in diatom skeletons; this might provide valuable clues about the mechanism.

**3.3. Structure at High Density ($\rho^* > 0.1$).** We now consider the characteristic structural lengthscales that develop in the model systems at moderate densities, $\rho^* > 0.1$. Of primary interest is the characteristic dimension of the cavities, that is to say, the spaces between the molecules, because this is where silica condensation would be most likely to occur. To gauge the dimensions of the cavities, we computed the static structure factor, which is sensitive to variations in density, and is accessible in scattering experiments.[45] The low-wavevector behavior of $S(q)$ was monitored by a direct calculation using the relation

$$S(\mathbf{q}) = \frac{1}{N_b}\langle \rho_{\mathbf{q}} \rho_{-\mathbf{q}} \rangle \tag{7}$$

where

$$\rho_{\mathbf{q}} = \sum_{j=1}^{N_b} \exp(-i\mathbf{q}\cdot\mathbf{r}_j) \tag{8}$$

is a Fourier component of the bead density, and $\mathbf{q}$ is a wavevector commensurate with the cubic periodic boundary conditions. Contributions with equal $q = |\mathbf{q}|$ were averaged.

In Figure 6 we show $S(q)$ at two densities ($\rho^* = 0.3$ and $\rho^* = 0.5$) and two temperatures ($T^* = 0.5$ and $T^* = 0.8$). At $\rho^* = 0.3$ and at both temperatures, peaks in $S(q)$ are visible in the region of $q \simeq 0.5\sigma^{-1}$. At $\rho^* = 0.5$ and $T^* = 0.5$, $S(q)$ continues to rise down to the lowest accessible wavevector ($q = 2\pi/L$) signaling that there is structure which spans the simulation cell. At $\rho^* = 0.5$ and $T^* = 0.8$, a peak is apparent at $q \simeq 1\sigma^{-1}$. $S(q)$ is a measure of inhomogeneity in the bead density on the lengthscale $2\pi/q$, and so the peaks in $S(q)$ signal the presence of structural features with that characteristic dimension. As we will confirm below, these structural features are the *voids*. With $\sigma \simeq 2$ nm, peaks in $S(q)$ at $q = 0.5-1\sigma^{-1}$ correspond to real-space dimensions in the range 13−25 nm. These dimensions are the same order of magnitude as those of the silica building blocks found in diatom skeletons.[4−8]

We now characterize the structure further by measuring a probability density of cavity sizes, $Q(r)$: the probability that the nearest bead to a randomly chosen point is at a distance between $r$ and $r + dr$ is $Q(r)dr$. (We note that $Q(r)$ is related to the excess chemical potential of a hard sphere immersed in the fluid.[46,47]) Every 20 time steps in the BD simulations, $N$ randomly selected points within the simulation cell were chosen, and a histogram of $Q(r)$ was accumulated.

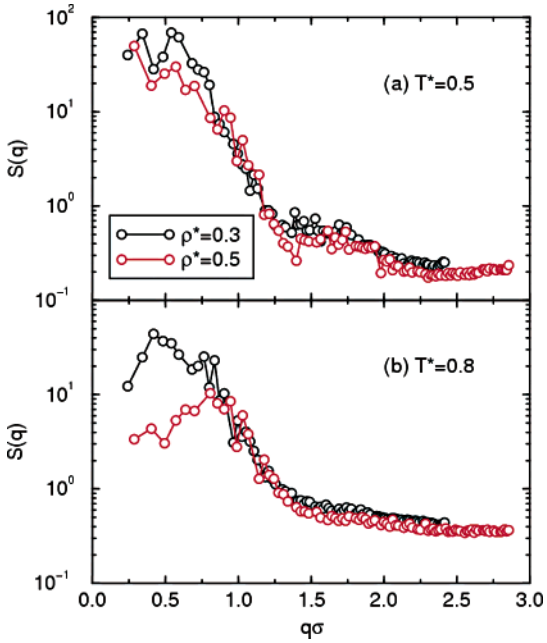


***Figure 6.*** Bead static structure factor, $S(q)$, at temperatures (a) $T^* = 0.5$ and (b) $T^* = 0.8$. The black points are at density $\rho^* = 0.3$, and the red points are at $\rho^* = 0.5$.

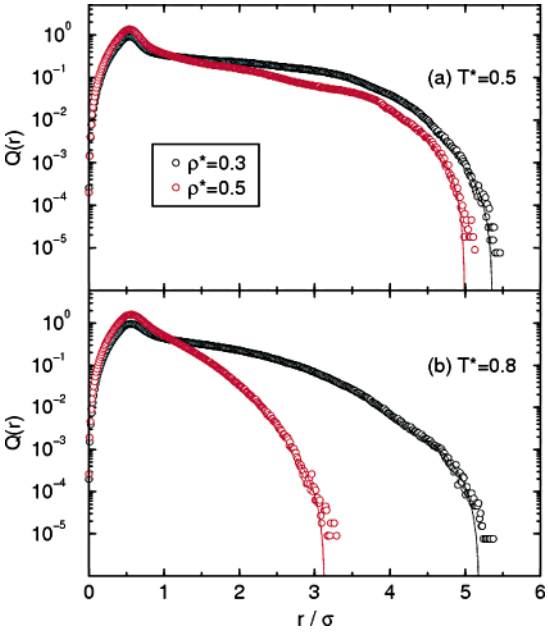


***Figure 7.*** Cavity-radius probability distribution function, $Q(r)$, at temperatures (a) $T^* = 0.5$ and (b) $T^* = 0.8$. The black points are at density $\rho^* = 0.3$, and the red points are at $\rho^* = 0.5$. The solid lines are fits to the assumed asymptotic form at large $r$, $Q(r) \propto (r_{max} - r)^2$, where $r_{max}$ is the maximum cavity radius.

A selection of results at densities $\rho^* > 0.1$, and temperatures $T^* = 0.5$ and $T^* = 0.8$, are shown in Figure 7. At all densities and temperatures, there are peaks in $Q(r)$ at $r \simeq 0.5\sigma$, which correspond to small cavities within regions of closely associated molecules. More significantly, peaks and shoulders at larger values of $r$ reflect the dimensions of the voids apparent in the simulation snapshots (Figure 2). We suggest that the most relevant lengthscale for biomineralization is the value of $r$ above which $Q(r)$ is essentially zero, since this should reflect the

(45) Chaikin, P. M.; Lubensky, T. C. *Principles of condensed matter physics;* Cambridge University Press: Cambridge, 1995.
(46) Pohorille, A.; Pratt, L. R. *J. Am. Chem. Soc.* **1990**, *112*, 5066−5074.
(47) Pratt, L. R.; Pohorille, A. *Proc. Natl. Acad. Sci. U.S.A.* **1992**, *89*, 2995−2999.

*maximum* dimensions of the cavities; to highlight the decay of $Q(r)$ at large $r$, the plots in Figure 7 are on linear−log scales. If the cavities are roughly spherical, then the probability of picking a point such that the distance from the inner surface of the cavity is between $r$ and $r + dr$ should scale like $4\pi(r_{max} - r)^2 dr$, i.e., $Q(r) \propto (r_{max} - r)^2$ as $r \rightarrow r_{max}$. This function was fitted to the data near $r_{max}$; the fits are included in Figure 7. As is clear from the figure, the values of $r_{max}$ lie in the range $3-6\sigma$, which corresponds to cavity diameters in the range 12−24 nm. These values match up very closely with those determined from $S(q)$ above, which shows that $S(q)$ and $Q(r)$ provide consistent measures of the cavity dimensions.

At these relatively high volume fractions (15−25%) silica growth would be controlled by the available space between the organic molecules. Hence, the cavities represent a kind of template. The resulting composite of silica and peptide might be the "moldable biosilica" from which certain (nonporous) structural elements of diatom skeletons are made.[20]

## 4. Conclusions

In this article, we have studied the structure of model peptides in aqueous solution using coarse-grained, Brownian dynamics computer simulations. The model peptides were constructed to mimic silaffins comprising 15 hydrophilic amino acids and two pendant long-chain polyamine tails. Effective attractive forces operated between the tails to represent either hydrophobic interactions (possibly more relevant to high-pH conditions) or phosphate-bridging between protonated nitrogen centers.

At low volume fractions (≤5%) distinct clusters are in evidence, with the mean separation between clusters being in the range 20−45 nm, depending on concentration. A gel-like structure emerges at a volume fraction of 15% in which a network of self-assembled strands spans the simulation cell, whereas at a volume fraction of 25%, the strands merge to form a more concentrated bicontinuous structure. The characteristic feature of these denser phases is the presence of cavities, with dimensions in the range 12−25 nm. The simulations are performed using reduced units, so there are uncertainties in our estimates of real dimensions. Nonetheless, despite the primitive nature of the peptide model, the characteristic structural length-scales are directly comparable with the dimensions of the moldable silica building blocks that fuse together to form diatom skeletons.

We suggest two different scenarios for the production of the moldable silica−peptide composite, each relevant to a different range of peptide concentration. At low peptide volume fractions (<5%) distinct aggregates could provide nucleation surfaces from which amorphous silica spheres might expand radially. A similar scenario has been put forward already by Patwardhan et al.[27] Roughly speaking, the apparent silica-sphere diameter would be delimited by the mean cluster separation. At higher volume fractions (>5%) growing amorphous silica blocks would be confined by the surrounding peptide network. To discriminate between the two scenarios, it is crucial to know how peptides are distributed within biosilica, and at what concentrations; this might be achieved using high-resolution microscopies (AFM, SEM, TEM). In the low-density nucleation scenario, the peptide would be concentrated in the cores of the silica blocks. In the high-density confinement picture, the peptide would be distributed more evenly, like a scaffold. We note here that, as a general rule, the volume fraction of macromolecules in a typical biological cell is of the order of 10%.[48] Alternatively, a volume fraction of ∼10% might be representative of the *local* peptide concentration in the interior of large aggregates, or indeed a compartment of the cell. During the growth process, the silica would eventually envelope the underlying peptide matrix, possibly resulting in a moldable composite with superior mechanical properties; knock-on effects of the growing silica on the templating peptide have not been examined here, but this may be examined in future work. The general principles suggested in this work may also apply to other systems, such as peptide R5[9,21−23] and poly(L-lysine).[27,17] Simulations might also be directed toward the effects of peptide conformation on the deposition of silica. Recent experiments show that poly(L-lysine) assembled into α-helices can pack into hexagonal sheets and hence template the formation of hexagonal silica platelets.[49] If converted to a $\beta$-sheet conformation, however, poly(L-lysine) deposits networks of silica spheres. To tackle these types of problems, a less coarse-grained simulation model is required to render variations in hydrophobicity and hydrophilicity within, say, a peptide backbone. We are currently working on calculations along these lines.

Finally, we speculate more generally on the roles of long-chain polyamines and silaffins in biomineralization. Long-chain polyamines in water likely form microemulsions of small droplets; indeed, this is the basis for the "phase separation" model proposed by Sumper.[16] Although this might lead to hierarchical patterning, it does not necessarily explain the fine structure of biosilica on the 10−100 nm scale. It is therefore conceivable that the role of the peptide backbones in silaffins is to frustrate microphase separation of the polyamine tails, and to promote local ordering on the molecular scale. This could be tested by analyzing silica deposition as a function of polyamine chain length and/or backbone hydrophilicity; longer chains and less-repulsive backbone groups should favor phase separation over self-assembly.[50]

This discussion is necessarily speculative. Nonetheless, we have made some concrete predictions which could be tested in a relatively straightforward way. In addition, we hope that our suggestions motivate a rational approach to designing silaffin analogues with useful structure-directing properties.

**Acknowledgment.** We thank Drs. Perdita Barran and David Dryden for discussions and critical readings of the draft manuscript, and the School of Chemistry at the University of Edinburgh for the provision of a studentship to L.L.

JA061211S

(48) Goodsell, D. S. *Trends Biol. Sci.* **1991**, *16*, 203−206.
(49) Patwardhan, S. V.; Maheshwari, R.; Mukherjee, N.; Kiick, K. L.; Clarson, S. J. *Biomacromolecules* **2006**, *7*, 491−497.
(50) Salaniwal, S.; Kumar, S. K.; Panagiotopoulos, A. Z. *Langmuir* **2003**, *19*, 5164−5168.